Advances in Water Resources 37 (2012) 86–93

Contents lists available at SciVerse ScienceDirect

Advances in Water Resources

journal homepage: www.elsevier.com/locate/advwatres

Incomplete mixing and reactions with fractional dispersion

Diogo Bolster [a,*], Pietro de Anna [b], David A. Benson [c], Alexandre M. Tartakovsky [d]

[a] Environmental Fluid Mechanics Laboratories, Dept. of Civil Engineering and Geological Sciences, University of Notre Dame, Notre Dame, IN, USA
[b] Géosciences Rennes, UMR 6118, CNRS, Université de Rennes 1, Rennes, France
[c] Hydrologic Science and Engineering, Colorado School of Mines, Golden, CO, USA
[d] Computational Mathematics Group, Pacific Northwestern National Laboratory, Richland, WA, USA

ARTICLE INFO

Article history:
Received 12 July 2011
Received in revised form 4 November 2011
Accepted 10 November 2011
Available online 23 November 2011

Keywords:
Fractional dispersion
Reactions
Incomplete mixing

ABSTRACT

A common barrier to accurately predicting the fate of reactive contaminants is accurately describing the role of incomplete mixing. In this paper we develop a stochastic analytical framework for an irreversible kinetic bimolecular reaction in a system with anomalous transport, governed by the fractional advection–dispersion equation (fADE). The classical well-mixed (thermodynamic) solution dictates that the concentration of reactants after an initial transient decreases proportional to t^{-1}. As the system becomes less and less well-mixed, the rate of reaction decreases relative to the thermodynamic solution, at late times scaling with $t^{-1/(2\alpha)}$ instead of t^{-1}, where $1 < \alpha \leqslant 2$ is the fractional order of the dispersion term in the fADE. The time at which this transition takes place is derived, giving an indication of the range of validity of the classical (well-mixed) equation. We verify these analytic results using particle-based simulations of random walks and reactions.

1. Introduction

Anomalous transport, or transport that does not follow Fick's Law of dispersive behavior, is common in a variety of hydrological and geophysical systems with heterogeneous velocity fields and typically arises due to nonlocal effects. Fields of interest where such anomalous behavior occurs include solute transport in surface [22] and subsurface water systems [33], turbulent environmental flows [12], sediment transport in rivers [8] and mechanical transport of soil constituents [19].

The classical 2nd-order advection–dispersion equation often cannot adequately model anomalous transport and a variety of mathematical models capable of doing so have emerged. Nonlocal effects can arise for a variety of reasons [11,32,13], but in short the concentration at some point should account for contributions from a variety of distances and/or the prior concentration history. Examples of the derivation of nonlocal methods in a variety of hydrological transport applications include delayed diffusion [15], projector formalisms [11], moment equations [32], multi-rate mass transfer [24], continuous time random walks [3] and fractional ADEs [40]. In this work we focus on the space-fractional ADE that is the continuum equation governing Lévy motion, which has been called ubiquitous [45]. The appeal lies in the fact that the model is sufficiently complex to display relevant dynamics while sufficiently simple to allow analytically tractable results that provide great insight into the influence of spatial nonlocality.

To date, the bulk of transport studies have focused on conservative transport. Many constituents of interest in hydrological systems do not behave conservatively, and their reactive character should be included, although predicting reactive transport in porous media can be quite challenging (see the recent review article by Dentz et al. [14]). Classical transport and reaction equations based on the assumption of perfect mixing fail to properly predict reactions within systems ranging from laboratory-scale in homogeneous material [36,23] to large-scale heterogeneous systems [29,47]. The deviations from classical reaction predictions can arise due to incomplete mixing [43,42], which must be accounted for in the correct upscaled model. For example, one might assume in an *ad hoc* manner that a kinetic reaction term is the result of upscaling the incomplete mixing process and arrive at accurate predictions of laboratory experiments (e.g. as done by [38] with the experiments of [23]).

Systems that can display anomalous transport for conservative constituents often display anomalous mixing characteristics (e.g., [37,9,46,5,28,27,4,10]). In some instances anomalous mixing can persist even when spreading of a conservative plume appears to be Fickian [28]. Such anomalous mixing in turn is expected to significantly impact chemical reactions where mixing is the mechanism that brings reactants together. The impact of anomalous transport on reactive systems of hydrological interest has to date received some attention (e.g., [6,16,17,47,29]). However, given the diverse nature of chemical reactions (e.g., instantaneous vs. kinetic, equilibrium, reversible vs. irreversible) a one-size-fits-all

* Corresponding author.
E-mail address: bolster@nd.edu (D. Bolster).

0309-1708/$ - see front matter © 2011 Elsevier Ltd. All rights reserved.
doi:10.1016/j.advwatres.2011.11.005

approach does not apply and interesting and important features arise depending on the specific type of reaction.

In this work we focus on irreversible kinetic reactions of the type $A + B \rightarrow C$. This is the simplest reactive system in which segregation or poor mixing of the species can lead to suppressed reactions. Therefore, the mechanics of transport and mixing bear directly on the ultimate reaction speed. For this system there is a competition between the rate of reaction between particles and the ability for A and B to mix by dispersive mechanisms. In a system that is continually well-mixed (say, as in a stirred beaker), the thermodynamic law follows

$$\frac{dC_A}{dt} = \frac{dC_B}{dt} = -kC_AC_B, \tag{1}$$

where C_i is the concentration of constituent i, and k [$L^d M^{-1} T^{-1}$] is the reaction rate coefficient. An especially interesting case is when the initial concentrations C_{A0} and C_{B0} are equal, then the solution to (1) is $C_A = C_B = C_{A0}(1 + C_{A0}kt)^{-1}$. It is important to note that these concentrations denote the ensemble average of a well-mixed process [20]. In a natural system that begins in an initially well-mixed state, the initial rate of reaction follows the thermodynamic law (1). The role of dispersive mechanisms in such a system is negligible (see [2,14]). However, as fluctuations of A or B become large with respect to the mean, isolated *islands* of A and B can form within which little or no reaction can occur, thus decreasing the rate at which the mean amount of A and B are consumed. This behavior was hypothesized and observed numerically for Fickian dispersion [35,26,44]. Using asymptotic arguments these authors showed that the rate of consumption of A and B changes from the initial thermodynamic value (which goes like t^{-1} after a brief initial time) to a rate that goes like $t^{-d/4}$, where d is the number of dimensions under consideration. It has subsequently been observed by other authors (e.g. [30,2,1]). This functional form of deviation from the thermodynamic law is valid for Fickian dispersion, but the deviation may be expected to be different in systems that do not display Fickian behavior.

Rather than rely on purely asymptotic arguments, we analytically derive solutions for the full time scaling of reaction rates associated with Lévy motion (including, as a subset, Brownian motion governed by Fick's Law). We do so using a stochastic model and the method of moments (e.g., [41,18]) and verify our results numerically with a particle-based reaction-dispersion model.

2. Model

Consider a system where two components A and B are distributed in space and can react chemically and irreversibly with one another. For simplicity we consider one-dimensional transport and reaction. The components are transported superdiffusively and are governed by the spatial fractional dispersion equation, so that

$$\frac{\partial C_i}{\partial t} = Dp\frac{\partial^\alpha C_i}{\partial x^\alpha} + Dq\frac{\partial^\alpha C_i}{\partial(-x)^\alpha} - kC_AC_B, \quad i = A, B, \tag{2}$$

where D [$L^\alpha T^{-1}$] is the dispersion coefficient, $1 \leqslant \alpha \leqslant 2$ is the fractional derivative exponent, and p and q are the weights of forward or backward dispersion, where $p + q = 1$ and $0 < p < 1$ (for symmetric dispersion $p = q = 0.5$). Mixing processes are given by both advective and dispersive mechanism. As a first step in understanding the impact of mixing on the global reaction rate, here we consider the case where the mixing processes are given only by fractional dispersion, neglecting the advective contribution. Note that the case of a constant advection term would cause a constant shift in time, but not affect mixing or reactions due to the principle of Gallilean invariance (i.e. the shift in the location of the center of mass is only affected by advection, while the rate of spreading of the plume around its center of mass, which influences mixing, is affected only by dispersion). In order to characterize the role incomplete mixing on the global chemical reaction rate, we focus on the dispersion-limited reaction case.

We begin by assuming that A and B are initially distributed in a uniformly random manner in a one-dimensional domain. This randomness persists, and we may decompose the random concentrations as $C_i(x,t) = \overline{C_i}(x,t) + C_i'(x,t), i = A, B$. The overbar refers to the ensemble average and the prime to fluctuations about this. We consider the initial average conditions:

$$\overline{C}_A(x,0) = \overline{C}_B(x,0) \equiv \overline{C}_{A0} \tag{3}$$

in an infinite domain with natural boundary conditions. Using (2) and the previous decomposition of concentration, the governing equations for the thermodynamic limit and the fluctuations from it can be written as

$$\frac{\partial \overline{C_i}}{\partial t} = -k\overline{C}_A\overline{C}_B - k\overline{C_A'C_B'} \tag{4}$$

and

$$\frac{\partial C_i'}{\partial t} = Dp\frac{\partial^\alpha C_i'}{\partial x^\alpha} + Dq\frac{\partial^\alpha C_i'}{\partial(-x)^\alpha} - k\overline{C}_AC_B' - kC_A'\overline{C}_B - kC_A'C_B' + k\overline{C_A'C_B'}, \tag{5}$$

where we used the fact that $\overline{C_i'} = 0$. We are interested in the evolution of $\overline{C}_i$, that depends on the evolution of the correlation structure of the local fluctuations. If both chemicals are initially distributed in the system through the same physical mechanism, it is reasonable to assume that the fluctuating components have initial identical correlation structure:

$$\overline{C_A'(x,0)C_A'(y,0)} = \overline{C_B'(x,0)C_B'(y,0)} = R(x,y). \tag{6}$$

Both A and B have similar initial correlation structures because the initial perturbations will arise due to small scale stochastic fluctuations (due to subscale noise/diffusion), which are expected to be similar for A and B as defined here.

A deviation from the thermodynamic law occurs when isolated patches of A and B emerge [44]. We select an initial condition for the fluctuation concentrations that reflects the emergence of such islands by taking A' and B' as initially anticorrelated such that

$$\overline{C_A'(x,0)C_B'(y,0)} = -R(x,y). \tag{7}$$

This is physically justifiable because in regions where there is an abundance of A relative to B, reactions will take place and result in a further depletion of B relative to the mean and excess of A relative to the mean. Similarly areas of excess B correspond to depleted A, thus giving rise to anti-correlation.

We can now write the equation for the covariance $f(x,y,t) = \overline{C_A'(x,t)C_B'(y,t)}$ as (see Appendix A)

$$\frac{\partial f(x,y,t)}{\partial t} = 2D\left(p\frac{\partial^\alpha f(x,y,t)}{\partial x^\alpha} + q\frac{\partial^\alpha f(x,y,t)}{\partial(-x)^\alpha}\right) \tag{8}$$

subject to initial condition $f(x, y, t = 0) = -R(x, y)$. The solution to (8) with natural boundary conditions on an infinite domain can be found with the Green's function, i.e.

$$f(x,y,t) = \int_{-\infty}^{\infty} -R(\xi,y)G(x,\xi,t)d\xi, \tag{9}$$

where

$$G(x,\xi,t) = \frac{1}{2\pi}\int_{-\infty}^{\infty} e^{2D[p(ik)^\alpha + q(-ik)^\alpha]t}e^{ik(x-\xi)}dk. \tag{10}$$

Because the initial correlation structure acts over a short range, we do not expect the specific initial correlation structure to play a major role. For simplicity we consider the limiting case of a delta correlated initial condition for f, i.e.

$$f(x,y,t=0) = -R(x,y) = -\sigma^2 l\delta(x-y), \tag{11}$$

where σ^2 is the variance and l the correlation length. This can be thought of as an approximation of an exponential or Gaussian correlation and it is straightforward to show that after some initial transient the solution for the delta correlation displays the same behavior (see Appendix B). In other studies it has been shown to give asymptotically similar results as short range correlation functions [34,7]. We are ultimately interested in the limit $y \to x$ and with the delta initial condition the solution for $f(x, y, t)$ is

$$\begin{aligned} f(x,y\to x,t) &= -\frac{\sigma^2 l}{2\pi}\int_{-\infty}^{\infty} e^{2D[p(ik)^\alpha + q(-ik)^\alpha]t}dk \\ &= -\frac{\sigma^2 l}{2\pi}t^{-1/\alpha}\int_{-\infty}^{\infty} e^{2D[p(im)^\alpha + q(-im)^\alpha]}dm = -\chi t^{-1/\alpha}, \end{aligned} \tag{12}$$

where $\chi = \frac{\sigma^2 l}{2\pi}\int_{-\infty}^{\infty} e^{2D[p(im)^\alpha + q(-im)^\alpha]}dm$ is a constant. Interestingly, the time scaling for f only depends on α, the fractional dispersion coefficient. Substituting (12) into (4) our equation for the mean concentration of A or B becomes

$$\frac{\partial \overline{C_i}}{\partial t} = -k\overline{C_i}^2 + k\chi t^{-1/\alpha}. \tag{13}$$

Strictly speaking, as written, Eq. (13) is not valid from time $t = 0$ as one has singular and nonphysical behavior associated with the term $k\chi t^{-1/\alpha}$. This problem is circumvented by accepting that this equation is only strictly valid after some initial "setting" time t_0 and defining the initial condition at this time such that $\overline{C}_A(t = t_0) = \overline{C}_{A0}$. It is equivalent to having an initial transient period during which the initial correlation and anticorrelation structure forms. We find that the solutions are insensitive to this small time [41].

3. Solution – discussion and implications

We will now work in nondimensional space. We nondimensionalize concentrations by the initial $\overline{C_{A0}}$ and time by $k\overline{C_{A0}}$ so that (13) can be written as

$$\frac{\partial \overline{C_i}}{\partial t} = -\overline{C_i}^2 + \chi^* t^{-1/\alpha} \quad \overline{C_A}(t = t_0) = 1, \tag{14}$$

where

$$\chi^* = \chi k^{\frac{1}{\alpha}}(C_{A0})^{\frac{1}{\alpha}-2} \tag{15}$$

$\chi^*$and α are now the only dimensionless numbers that play a role in this system. Note that the right side of (14) has a sink and a source term. At early time the well-mixed (first) term dominates, but at late time the well-mixed sink is balanced by the "source" that accounts for imperfect mixing.

3.1. Well mixed system (thermodynamic limit)

A well mixed system can be represented by $\chi^* = 0$. This is equivalent to the classical thermodynamic limit equations where the fluctuations in concentrations are zero, i.e.

$$\frac{\partial \overline{C_i}}{\partial t} = -\overline{C_i}^2 \quad \overline{C_A}(t = t_0) = 1. \tag{16}$$

The solution to this equation is well known and given by

$$\overline{C_A}(t) = \frac{1}{1 + (t - t_0)}. \tag{17}$$

In particular it is worth noting that at large times the concentration of A scales inversely with time, i.e. $\overline{C_A}(t) \sim t^{-1}$.

3.2. Incomplete mixing

We now look at the full solution of Eq. (14) accounting for the source terms that quantifies incomplete mixing. Eq. (14) is a Riccati equation and has solution

$$\overline{C_i}(t) = \frac{\sqrt{\chi^*}}{t^{\frac{1}{2\alpha}}}\frac{\left(I_{-\frac{\alpha-1}{2\alpha-1}}(z) - \kappa K_{\frac{\alpha-1}{2\alpha-1}}(z)\right)}{\left(I_{\frac{\alpha}{2\alpha-1}}(z) + \kappa K_{\frac{\alpha}{2\alpha-1}}(z)\right)}, \quad z = \frac{2\alpha\sqrt{\chi^*}}{2\alpha-1}t^{\frac{2\alpha-1}{2\alpha}}, \quad t \geqslant t_0, \tag{18}$$

where the I and K are modified Bessel functions of the first and second kind and κ is a constant that depends on the initial condition and is given by

$$\kappa = \frac{\left(I_{-\frac{\alpha-1}{2\alpha-1}}(z_0) - \chi^{*\frac{-1}{2}}t_0^{\frac{1}{2\alpha}}I_{\frac{\alpha}{2\alpha-1}}(z_0)\right)}{\left(K_{\frac{\alpha-1}{2\alpha-1}}(z_0) + \chi^{*\frac{-1}{2}}t_0^{\frac{1}{2\alpha}}K_{\frac{\alpha}{2\alpha-1}}(z_0)\right)}, \quad z_0 = \frac{2\alpha\sqrt{\chi^*}}{2\alpha-1}t_0^{\frac{2\alpha-1}{2\alpha}}. \tag{19}$$

3.3. Early time

At first glance the analytical solution in (18) may not appear to give much insight. However, early and late time expansions of this solution clarify the situation significantly. To leading order, at early time the solution in (18) is given by

$$\overline{C_A}(t) = \frac{1}{1 + (t - t_0)}, \tag{20}$$

which is identical to the well-mixed thermodynamic solution (Fig. 1) and shows consistency of the solution with an assumption of early conditions that are sufficiently mixed for the thermodynamic rate to dominate. If this thermodynamic solution held at all times one would expect a late time scaling that goes like inverse time, i.e., t^{-1}.

3.4. Late time

At late time, the fraction in parentheses in Eq. (18) containing the Bessel functions converges to unity, and the leading order behavior becomes

$$\overline{C_A}(t) \sim \sqrt{\chi^*}t^{-1/(2\alpha)}. \tag{21}$$

Unlike the thermodynamic solution, which scales as t^{-1}, the solution of (18) decreases at a slower rate of $t^{-1/(2\alpha)}$ (Fig. 1). For the Fickian case of $\alpha = 2$ this results in a late time scaling of $t^{-1/4}$, in agreement with previous predictions and observations (e.g. [35,26,44,2,1]).

3.5. Cross-over time

In the above discussion we talk about early and late times without clearly defining these. On physical grounds we define early times as times when the thermodynamic law still holds and late times as times when the anomalous kinetics emerge. The cross-over time that delineates early and late times can be found by balancing both terms on the right hand side of (14); i.e., it is when the terms that reflect well-mixed conditions and imperfectly mixed conditions become comparable in size. Thus we can define a dimensionless cross-over time τ such that $\frac{1}{\tau^2} = \chi^*\tau^{-1/\alpha}$. Solving for τ we obtain

$$\tau = \chi^{*\frac{\alpha}{1-2\alpha}}. \tag{22}$$

When $t > \tau$, anomalous kinetics are expected and at early time, when $t < \tau$, behavior consistent with the thermodynamic law is observed. The larger the value of χ^*, the earlier the onset of

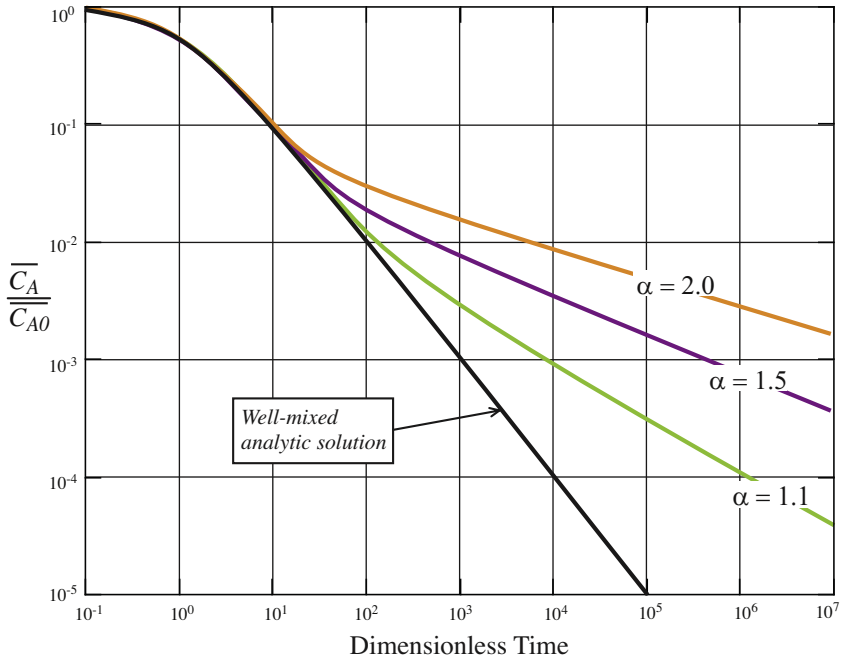

Fig. 1. Plots of the analytical solution (18) for a variety of values of α: 1.1, 1.5, and 2.0. Note that in all cases the solution pulls away from the well-mixed thermodynamic limit (black solid line) and at late times scales like $t^{-1/(2\alpha)}$. Each solution uses a value of $\chi^* = 0.005$.

anomalous kinetics. Recall that χ^* is a dimensionless number that reflects how noisy the initial concentration field is, as well as the competition between diffusion and reaction time scales. For illustration let us consider the Fickian case of $\alpha = 2$. Here

$$\chi^* = \sqrt{\frac{1}{8\pi}}\frac{\sigma^2}{C_{A0}^2}\sqrt{\frac{kl^2 C_{A0}}{D}}, \tag{23}$$

which is closely related to the (dimensionless) dispersive Damkohler number $Da = \tau_D/\tau_R = kl^2 C_{A0}/D$ (e.g. [39]). The Damkohler number is a ratio of the time scale of diffusion $\tau_D = l^2/D$ to the time scale of reaction $\tau_R = 1/kC_{A0}$, thereby quantifying how quickly reactions occur relative to dispersion. Our dimensionless χ^* is proportional to Da^2, with the constant of proportionality including a term $\frac{\sigma^2}{C_{A0}^2}$ that reflects the amplitude of initial "noise" in the distribution of A and B. An increase in Da means that reactions are faster relative to the rate of diffusion and the system has a quicker onset of incomplete mixing; i.e., A and B are consumed quickly relative to how quickly diffusion can bring them together. The additional term accounts for the smoothness in the initial condition, which directly affects that time of the onset of separate A and B islands and incomplete mixing.

4. Numerical simulations

To verify the theoretical results, we simulated random walks and particle/particle reactions using the method of [2] modified for Lévy motion. The details of the algorithm are given in [2] and the modified version is briefly outlined here. Time is discretized into steps of identical duration Δt. Each particle jumps a random distance in the domain of attraction (DOA) of an α-stable law (i.e. by the generalized central limit theorem they additively converge to an α-stable distribution [21]) so that the random walk approximates Lévy motion. We also must rapidly calculate the probability density of the sum of two random walks to estimate the probability that two particles will be co-located and potentially react. Therefore, we require jumps for which random values are easy to generate and the density function is also easy to calculate (effectively ruling out α-stable random variables themselves).

Due to the power-law tails, the shifted Pareto distribution $P(|X| > x) = s^\alpha(x+s)^{-\alpha}$ [25] is in the domain of attraction of the α-stable laws (by the generalized central limit theorem); therefore, a sum of random jumps drawn from this distribution will converge to Lévy motion. This is analogous to summing variables from a uniform distribution to simulate a Brownian motion by invoking the classical central limit theorem. However, relative to the corresponding α-stable density, the shifted Pareto density is too peaked at the origin and nearby particles are too likely to react. Instead we choose symmetric jumps X from a "chopped" Pareto (see for example Fig. 2) distribution following

$$P(|X| < x) = \begin{cases} mx & \text{if } x < ((1+\alpha)c)^{1/\alpha}, \\ 1 - cx^{-\alpha} & \text{otherwise.} \end{cases} \tag{24}$$

The constants c and m dictate the size of the jumps. Both c and m are functions of Δt and D. Each jump should be DOA α-stable with scale $(D\Delta t)^{1/\alpha}$, so that by (7.19)–(7.21) in [31], $c = D\Delta t/(\Gamma(1-\alpha)\cos(\pi\alpha/2))$. The slope m and cutoff $((1+\alpha)c)^{1/\alpha}$ are chosen to ensure a mono-modal density by making the small x uniform cumulative distribution tangent to the power law with prefactor c. The form we chose for this jump density is one that most closely approximates an α-stable variable, while still being computationally efficient. For $\alpha \geqslant 2$, the jumps are in the domain of attraction of a Gaussian and simpler traditional methods can be used. The separate probability density, denoted $v(s)$, that two particles will be co-located in any time interval given initial separation s is the convolution of two α-stable densities with each other. This is also α-stable. We use the chopped Pareto to calculate the density that approximates the α-stable law with scale $(2D\Delta t)^{1/\alpha}$.

An initial number N_0 of both A and B particles are (uniformly) randomly placed in a $1-D$ domain of size Ω. Note that we do not impose the initial conditions in equations (6) and (7) as done in the theory. Rather, we allow the randomness to naturally evolve from the uniform initial condition at $t = 0$. This evolution reflects the initial 'setting time' discussed in Section 2. The reactions are

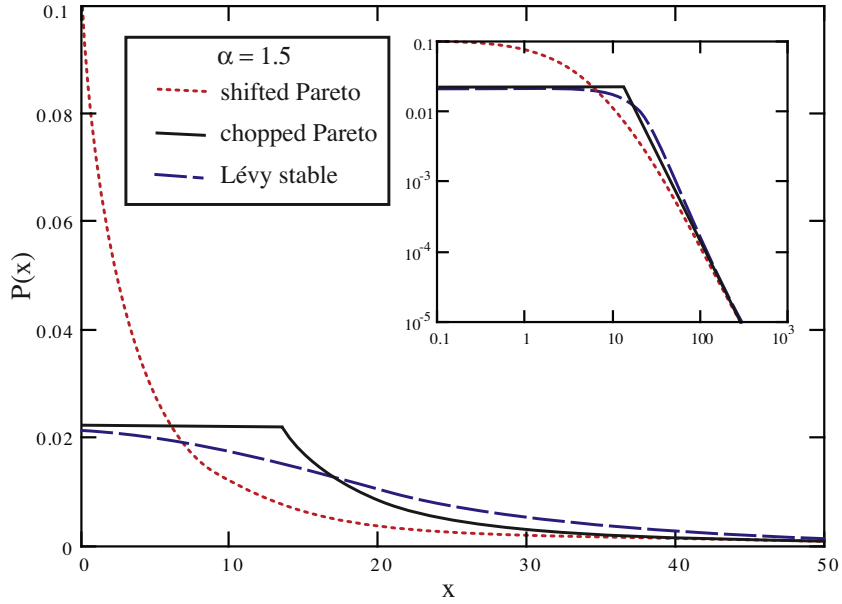

Fig. 2. Densities for random variables in the domain of attraction of a Lévy-stable with index $\alpha = 1.5$. Scale $(D\Delta t)^{1/\alpha} = 13.6$.

simulated by calculating the probability density of particle co-location ($v(s)$) by Lévy dispersion. This probability is multiplied by the thermodynamic probability of reaction given the co-location. Each particle represents a total mass $\Omega\overline{C_{A0}}/N_0$, so the probability of reaction [2] is $k\Delta t(\Omega\overline{C_{A0}}/N_0)v(s)$. This probability for each A and B particle pair is compared to a new Uniform(0, 1) random variable until a reaction takes place or pairs are exhausted. The particles then diffuse by random walks and react again *ad nauseum*.

In all of the Lagrangian simulations, the reaction rate follows the well-mixed solution until the late time scaling sets in. In agreement with our theoretical development, the late time solution scales with $t^{-1/(2\alpha)}$ (Fig. 3). Each simulation used representative values for aqueous environments: domain size $\Omega = 200$ cm; $\overline{C_{A0}} = \overline{C_{B0}} = 0.001$ and $k = 1.0$, where the latter two constants use consistent concentration units. The dispersion coefficients were varied to get ample separation of data points for visual clarity: For $\alpha = 1.1$, 1.5, and 2.0, $D = 5 \times 10^{-6}$, 2.5×10^{-6}, and 1×10^{-6} cm$^{\alpha}$/s, respectively. The initial number of both A and B particles was 20,000; each simulation was run 40 times and the ensemble average concentrations were calculated. Even single realizations display the anomalous behavior clearly and 40 were chosen to smooth any existing noise. Doubling the number of realizations does not appear to change the solution and so 40 realizations are deemed sufficient.

At the latest time in the numerical simulations, another (approximately exponential) scaling arises that is not predicted by our analytical development. This deviation from the theoretical

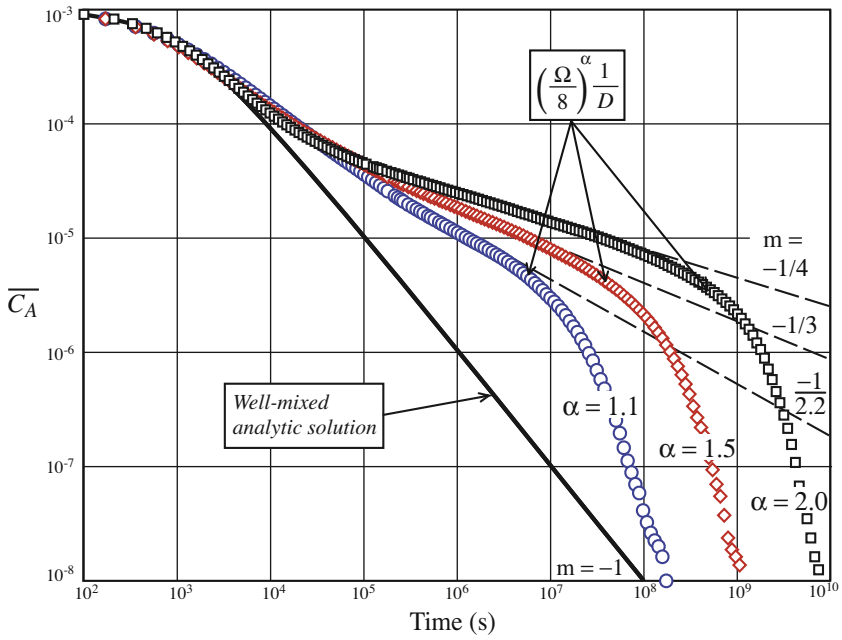

Fig. 3. Concentration change simulated by particle models (symbols) and analytic solutions to well-mixed equation (solid curve). All solutions transition from the perfectly mixed solution of to the $t^{-1/(2\alpha)}$ asymptotic solution. The approximate time $(\Omega/8)^{\alpha}/D$ at which the boundaries are felt, on average, is denoted on the plots.

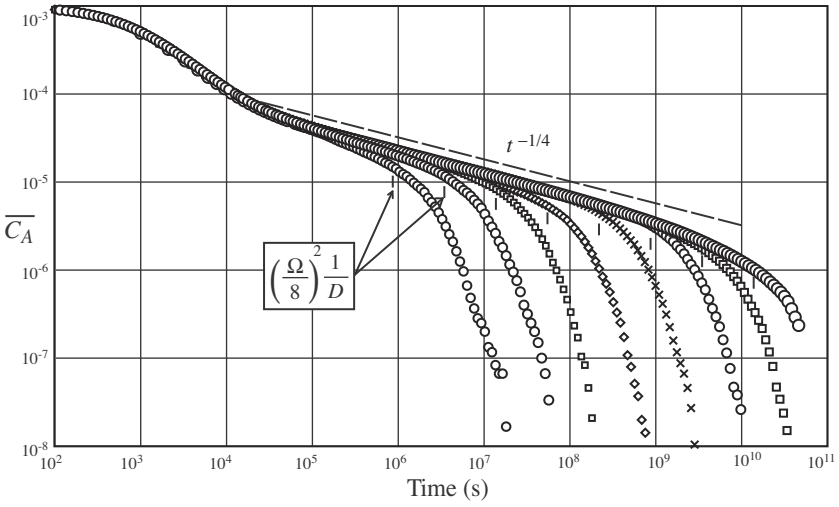

Fig. 4. Effect of finite-sized domains on Brownian motion dispersion ($\alpha = 2$) and reactions. Each simulation is identical except for a doubling of domain size, which theoretically quadruples the time at which boundaries impede segregation of A and B into separate islands. The theoretical transition time $(\Omega/8)^\alpha/D$ at which the boundaries are felt, on average, is denoted by vertical ticks.

prediction can be attributed to the finite size of the computational domain and the fact that the theoretical development is for an infinite medium. While one might expect that the boundaries would increase reaction rates at all times because of the very large (inter-island) distances that the particles may take at any time, it is the average size of the islands that dictates the late-time transition back to well-mixed rates (Fig. 3). A simple argument shows that the islands grow at a Lévy diffusive rate of $(Dt)^{1/\alpha}$, so that the fringes of the largest island may feel the boundary at time $t = (\Omega/K)^\alpha/D$, where K is some empirical constant that describes the distance out along an island where the reactions are taking place. We find that a value of $K = 8$ is a reasonable guide to the onset of boundary effects (Fig. 3). To demonstrate that this is truly a boundary effect and test this approximation, we ran the simulations for Fickian dispersion and reaction as shown in Fig. 4. In this case the ratio of the initial number of particles to the domain size is fixed at $N_0/\Omega = 40$ so that the average particle spacing is the same for any domain size. The domain size is doubled successively, which increases by a factor of four the time at which the boundaries are felt by the reaction (Fig. 4).

5. Conclusions

The role of incomplete mixing greatly complicates the accurate predictions of effective chemical reaction rates. Not only is the overall rate different from the well-mixed case, but the functional form is different, pointing to the insufficiency of the classical (thermodynamic) rate equation. We showed, for a simple set of cases, how the correct ensemble concentration evolution equation can be derived using stochastic analytic methods. In particular, as incomplete mixing effects dominate, the rate of decay of chemical species changes from t^{-1} to $t^{-1/(2\alpha)}$, which for the Fickian case of $\alpha = 2$ is consistent with previous observations [2,1]. Enhanced dispersion leads to faster decay than the Fickian counterpart, but the system is still slowed and dispersion-limited relative to the well-mixed system.

The mechanics of the underlying dispersion and mixing process is directly incorporated into the ensemble governing equation through the action of the fractional dispersion Green function on the initial degree of imperfect mixing in the system. This analysis leads to a dimensionless number that marks the transition from good mixing and the classical governing equation to poor mixing and the equation with a new term. Analytic arguments also show the time at which the domain boundaries destroy the poor mixing by limiting the size of the islands that are enriched in one or the other reactant.

The work here focuses purely on the role of fractional dispersion on incomplete mixing and reactions. However, the methodologies (both analytic and numerical) developed here are quite general and should allow for the analyses of more complicated and realistic geometries and mixing mechanisms. Incorporating the small scale mixing limitations imposed by heterogeneous velocity fields and local dispersion within larger scale reaction predictions is of significant practical interest to the water resources community as a whole.

Acknowledgements

Diogo Bolster would like to express thanks for financial support from NSF via Grant EAR-1113704. David Benson would like to express thanks for financial support from NSF via Grants EAR-0749035 and DMS-0539176 and the Department of Energy through Grant DOE DE-FG02-07ER15841. Any opinions, findings, conclusions, or recommendations do not necessarily reflect the views of the funding agencies. Pietro de Anna would like to express thanks for the financial support of the European Commission through FP7 project, IMVUL (Grant Agreement 212298). Alexander Tartakovsky was partially supported by the Office of Advanced Scientific Computational Research of the Department of Energy.

Appendix A. Covariance equation

Multiplying (5) for $i = A$ by $C'_B(y)$ and discarding terms of higher than second order in fluctuations we obtain

$$C'_B(y)\frac{\partial C'_A(x)}{\partial t} = D\left(p\frac{\partial^\alpha C'_A(x)C'_B(y)}{\partial x^\alpha} + q\frac{\partial^\alpha C'_A(x)C'_B(y)}{\partial(-x)^\alpha}\right) - k\overline{C_A(x)}C'_B(x)C'_B(y) - k\overline{C_A(x)}C'_A(x)C'_B(y). \quad (A.1)$$

Similarly multiplying (5) for $i = B$ by $C'_A(y)$ and discarding terms of higher than second order in fluctuations we obtain

$$C'_A(y)\frac{\partial C'_B(x)}{\partial t} = D\left(p\frac{\partial^\alpha C_B(x)C'_A(y)}{\partial x^\alpha} + q\frac{\partial^\alpha C'_B(x)C'_A(y)}{\partial(-x)^\alpha}\right) - k\overline{C_B(x)}C'_A(x)C'_A(y) - k\overline{C_B(x)}C'_B(x)C'_A(y). \quad (A.2)$$

Taking the ensemble average of (A.1) and (A.2) and recognizing that by stationarity $\overline{C'_B(y)C'_A(x)} = \overline{C'_A(y)C'_B(x)}$, we sum the equations and obtain the following equation for the covariance

$$\overline{C'_B(y)\frac{\partial C'_A(x)}{\partial t} + C'_A(y)\frac{\partial C'_B(x)}{\partial t}} = 2D\left(p\frac{\partial^\alpha \overline{C'_A(x)C'_B(y)}}{\partial x^\alpha} + q\frac{\partial^\alpha \overline{C'_A(x)C'_B(y)}}{\partial(-x)^\alpha}\right) - 2k\overline{C_A(x)C'_A(x)C'_A(y)} - 2k\overline{C_A(x)C'_A(x)C'_B(y)}, \quad (A.3)$$

which can be rewritten as

$$\frac{\partial \overline{C'_A(x)C'_B(y)}}{\partial t} = 2D\left(p\frac{\partial^\alpha \overline{C'_A(x)C'_B(y)}}{\partial x^\alpha} + q\frac{\partial^\alpha \overline{C'_A(x)C'_B(y)}}{\partial(-x)^\alpha}\right) - 2k\overline{C_A(x)C'_A(x)C'_A(y)} - 2k\overline{C_A(x)C'_A(x)C'_B(y)}. \quad (A.4)$$

Similarly, an equation for $\overline{C'_A(x)C'_A(y)}$ is given by

$$\frac{\partial \overline{C'_A(x)C'_A(y)}}{\partial t} = 2D\left(p\frac{\partial^\alpha \overline{C'_A(x)C'_A(y)}}{\partial x^\alpha} + q\frac{\partial^\alpha \overline{C'_A(x)C'_A(y)}}{\partial(-x)^\alpha}\right) - 2k\overline{C_A(x)C'_B(x)C'_A(y)} - 2k\overline{C_B(x)C'_A(x)C'_A(y)}. \quad (A.5)$$

Subtracting Eq. (A.5) from Eq. (A.4) gives:

$$\frac{\partial[\overline{C'_A(x,t)C'_B(y,t)} - \overline{C'_A(x,t)C'_A(y,t)}]}{\partial t} = 2D\left(p\frac{\partial^\alpha\left(\overline{C'_A(x)C'_B(y)} - \overline{C'_A(x)C'_A(y)}\right)}{\partial x^\alpha} + q\frac{\partial^\alpha\left(\overline{C'_A(x)C'_B(y)} - \overline{C'_A(x)C'_A(y)}\right)}{\partial(-x)^\alpha}\right). \quad (A.6)$$

As laid out in the main body of the text the initial conditions for these are

$$\overline{C'_A(x,0)C'_A(y,0)} = -\overline{C'_A(x,0)C'_B(y,0)} = R(x,y). \quad (A.7)$$

Therefore, from moment Eqs. (A.4) and (A.5) it follows that

$$\overline{C'_A(x,y,t)C'_B(x,y,t)} = -\overline{C'_A(x,y,t)C'_A(x,y,t)} \quad (A.8)$$

and with this is mind, we can rewrite the 1-D Eq. (A.6)

$$\frac{\partial[\overline{C'_A(x,t)C'_B(y,t)}]}{\partial t} = 2D\left(p\frac{\partial^\alpha\left(\overline{C'_A(x)C'_B(y)}\right)}{\partial x^\alpha} + q\frac{\partial^\alpha\left(\overline{C'_A(x)C'_B(y)}\right)}{\partial(-x)^\alpha}\right). \quad (A.9)$$

Appendix B. Alternative initial correlation structures

In this appendix we demonstrate that another short range correlation structure, namely the exponential, give the same long time behavior as the delta correlation, thus justifying its selection. Specify now:

$$f(x,y,t=0) = R(x,y) = -\sigma^2 e^{-\frac{|x-y|}{l}}. \quad (B.1)$$

Substituting into (9) for the limit of $y \to x$

$$f(x,y\to x,t) = -\frac{\sigma^2}{\pi}\int_{-\infty}^{\infty}\frac{l}{k^2l^2+1}e^{2D[p(ik)^\alpha]+q(-ik)^\alpha]t}dk = -\frac{\sigma^2}{\pi}\int_{-\infty}^{\infty}\frac{lt^{\frac{1}{\alpha}}}{m^2l^2+t^{\frac{2}{\alpha}}}e^{2D[p(im)^\alpha]+q(-im)^\alpha]}dm. \quad (B.2)$$

If we take the limit of long time ($t \to \infty$)

$$f(x,y\to x,t) \sim -t^{-1/\alpha}\frac{\sigma^2 l}{2}\int_{-\infty}^{\infty}e^{2D[p(im)^\alpha]+q(-im)^\alpha]}dm \quad (B.3)$$

which is the same scaling that arises for the delta initial correlation for all times. Similar results can be shown for other short range correlation structures such a Gaussian one.

References

[1] de Anna P, Le Borgne T, Dentz M, Bolster D, Davy P. Anomalous kinetics in diffusion limited reactions linked to non-Gaussian concentration PDF. J Chem Phys 2011;135:174104.

[2] Benson DA, Meerschaert MM. Simulation of chemical reaction via particle tracking: diffusion-limited versus thermodynamic rate-limited regimes. Water Resour Res 2008;44:W12201. doi:10.1029/2008WR007111.

[3] Berkowitz B, Cortis A, Dentz M, Scher H. Modeling non-Fickian transport in geological formations as a continuous time random walk. Rev Geophys 2006;44:RG2003.

[4] Bolster D, Dentz M, Le Borgne T. Hyper mixing in shear flow. Water Resour Res 2011;47:W09602. doi:10.1029/2011WR010737.

[5] Bolster D, Valdes-Parada FJ, Le Borgne T, Dentz M, Carrera J. Mixing in confined stratified aquifers. J Contam Hydrol 2011;120–121:P198–21. doi:10.1016/j.jconhyd.2010.02.003.

[6] Bolster D, Benson DA, LeBorgne T, Dentz M. Anomalous mixing and reaction induced by superdiffusive nonlocal transport. Phys Rev E 2010;82:021119. doi:10.1103/PhysRevE.82.021119.

[7] Bolster D, Dentz M, Carrera J. Effective two-phase flow in heterogeneous media under temporal pressure fluctuations. Water Resour Res 2009;45:W05408.

[8] Bradley D, Tucker G, Benson D. Fractional dispersion in a sand bed river. J Geophys Res F Earth Surf 2010;115:F00A09. doi:10.1029/2009JF001268.

[9] Chiogna G, Cirpka OA, Gratwohl P, Rolle M. Transverse mixing of conservative and reactive tracers in porous media: quantification through the concepts of flux-related and critical dilution indices. Water Resour Res 2011;47:W02505.

[10] Cirpka OA, de Barros FPJ, Chiogna G, Rolle M, Nowak W. Stochastic flux-related analysis of transverse mixing in two-dimensional heterogeneous porous media. Water Resour Res 2011;47:W06515.

[11] Cushman JH, Ginn TR. Nonlocal dispersion in media with continuously evolving scales of heterogeneity. Transport Porous Med 1993;13:123–38.

[12] Cushman-Roisin B. Beyond eddy diffusivity: an alternative model for turbulent dispersion. Environ Fluid Mech 2008;8:543–9.

[13] Dentz M, Bolster D. Distribution versus correlation-induced anomalous transport in quenched random velocity fields. Phys Rev Lett 2010;105:244301.

[14] Dentz M, LeBorgne T, Englert A, Bijeljic B. Mixing, spreading and reaction in heterogeneous media: a brief review. J Contam Hydrol 2011;120–121:1–17.

[15] Dentz M, Tartakovsky DM. Delay mechanisms of non-Fickian transport in heterogeneous media. Geophys Res Lett 2006;33(16):L16406.

[16] Donado LD, Sánchez-Vila X, Dentz M, Carrera J, Bolster D. Multicomponent reactive transport in multicontinuum media. Water Resour Res 2009;45:W11402.

[17] Edery Y, Scher H, Berkowitz B. Modeling bimolecular reactions and transport in porous media. Geophys Res Lett 2009;35:L02407.

[18] Fiori A, Jankovic I. Can we determine the transverse macrodispersivity by using the method of moments. Adv Water Resour 2005;28(6):589–99.

[19] Furbish D, Childs E, Haff P, Schmeeckle M. Rain splash of soil grains as a stochastic advection–dispersion process, with implications for desert plant–soil interactions and land-surface evolution. J Geophys Res 2009;114:F00A03.

[20] Gillespie DT. The chemical Langevin equation. J Chem Phys 2000;113(1):297–306.

[21] Gnedenko BV, Kolmogorov AN. Limit distributions for sums of independent random variables. Addison-Wesley; 1954 [Translated from Russian].

[22] Gooseff MN, Wondzell SM, Haggerty R, Anderson J. Comparing transient storage modeling and residence time distribution (RTD) analysis in geomorphically varied reaches in the Lookout Creek basin, Oregon, USA. Adv Water Resour 2003;26:925–37.

[23] Gramling C, Harvey CF, Meigs LC. Reactive transport in porous media: a comparison of model prediction with laboratory visualization. Environ Sci Technol 2002;36:2508–14.

[24] Haggerty R, Gorelick SM. Multiple-rate mass transfer for modeling diffusion and surface reactions in media with pore-scale heterogeneity. Water Resour Res 1995;31(10):2383–400.

[25] Van Hauwermeiren M, Vose D. A compendium of distributions. [ebook]. Ghent, Belgium: Vose Software; 2009.

[26] Kang K, Redner S. Fluctuation dominated kinetics in diffusion-controlled reactions. Phys Rev A 1985;32:435–47.

[27] Le Borgne T, Dentz M, Bolster D, Carrera J, de Dreuzy J-R, Bour O. Persistence of incomplete mixing: a key to anomalous transport. Phys Rev E 2011;84:015301(R).

[28] Le Borgne T, Dentz M, Bolster D, Carrera J, de Dreuzy J-R, Davy P. Non-Fickian mixing: temporal evolution of the scalar dissipation rate in porous media. Adv Water Resour 2010;33:1468–75.

[29] Luo J, Cirpka OA. How well do mean breakthrough curves predict mixing-controlled reactive transport? Water Resour Res 2011;47:W02520.

[30] Monson E, Kopelman R. Nonclassical kinetics of an elementary $A+B\to C$ reaction–diffusion system showing effects of a speckled initial reactant distribution and eventual self-segregation. Exp Phys Rev E 2004;69:021103.

[31] Meerschaert MM, Scheffler H-P. Limit distributions for sums of independent random vectors: heavy tails in theory and practice. Wiley Interscience; 2001.

[32] Neuman SP. Lagrangian theory of transport in space-time nonstationary velocity fields: exact nonlocal formalisms by conditional moments and weak approximation. Water Resour Res 1993;29:633–45.

[33] Neuman SP, Tartakovsky DM. Perspective on theories of anomalous transport in heterogeneous media. Adv Water Resour 2009;32:670–80.
[34] Neuweiler I, Attinger S, Kinzelbach W, King P. Large scale mixing for immiscible displacement in heterogeneous porous media. Transport Porous Med 2003;51:287–314.
[35] Ovchinnikov AA, Zeldovich YB. Role of density fluctuations in bimolecular reactions. Chem Phys 1978;28:215–8.
[36] Raje D, Kapoor V. Experimental study of bimolecular reaction kinetics in porous media. Environ Sci Technol 2000;34:1234–9.
[37] Rolle M, Eberhardt C, Chiogna G, Cirpka OA, Gratwohl P. Enhancement of dilution and transverse reactive mixing in porous media: experiments and model-based interpretation. J Contam Hydrol 2009;110:130–42.
[38] Sánchez-Vila X, Fernández-Garcia D, Guadagnini A. Interpretation of column experiments of transport of solutes undergoing an irreversible bimolecular reaction using a continuum approximation. Water Resour Res 2010;46: W12510.
[39] Sanchez-Vila X, Dentz M, Donado LD. Transport-controlled reaction rates under local non-equilibrium conditions. Geophys Res Lett 2007;34:L10404. doi:10.1029/2007GL029410.
[40] Schumer R, Meerschaert MM, Baeumer B. Fractional advection–dispersion equations for modeling transport at the earth surface. J Geophys Res 2009;114:F00A07.
[41] Tartakovsky AM, de Anna P, Borgne TL, Balter A, Bolster D. Effects of spatial concentration fluctuations on non-linear reactions. Water Resour Res [submitted for publication].
[42] Tartakovsky AM, Tartakovsky DM, Meakin P. Stochastic Langevin model for flow and transport in porous media. Phys Rev Lett 2008;101:044502.
[43] Tartakovsky AM, Tartakovsky GD, Scheibe TD. Effects of incomplete mixing on multicomponent reactive transport. Adv Water Resour 2009; 32:1674–9.
[44] Toussaint D, Wilczek F. Particle–antiparticle annihilation in diffusive motion. J Chem Phys 1983;78:2642–7.
[45] Tsallis C, Levy SVF, Souza AMC, Maynard R. Statistical–mechanical foundation of the ubiquity of the Lévy distributions in Nature. Phys Rev Lett 1996;77:5442.
[46] Werth CJ, Cirpka OA, Grathwohl P. Enhanced mixing and reaction through flow focusing in heterogeneous porous media. Water Resour Res 2006;42:W12414. doi:10.1029/2005WR004511.
[47] Willmann M, Carrera J, Sánchez-Vila X, Silva O, Dentz M. Coupling of mass transfer and reactive transport for nonlinear reactions in heterogeneous media. Water Resour Res 2010;44:W12437.